

Numerical Simulation and Experimental of Residual Stress Field of SAE1070 Spring Steel Induced by Laser Shock

Bing Han, Changliang Xu, Jialian Shi and Hua Song

School of Mechanical Engineering and Automation, University of Science and Technology
Liaoning, Anshan 114051, China

Abstract: Laser Shock Processing (LSP) is an innovative surface treatment technology. LSP can induce compressive residual stress layer in the surface of metallic materials, which is used for improving the fatigue life. In this study, the propagation course of typical laser shock wave in material was analyzed according to the theory of plasticity dynamics and the theory of stress wave. The effects of laser shock processing, residual stress of SAE1070 steel surface layer were studied. The finite element software ANSYS/LS-DYNA was applied to simulate the residual stress field of SAE1070 steel surface layer induced by laser shock processing. A bilinear isotropic model in a nonlinear inelastic model is created by using ANSYS/LS-DYNA finite element analysis software. Shock wave pressures under different peak loads are adopted to predict residual stress distribution. The experimental results for the magnitude and distribution of residual stress are consistent with the numerical simulation.

Keywords: Laser shock processing, residual stress, numerical simulation, finite element

INTRODUCTION

Laser Shock Processing (LSP) is a new surface modification technology. LSP is a process similar to traditional shot peening, in which favorably oriented compressive residual stresses are imparted at and near the surface of the target material. In the process of LSP the laser with high power density and burst pulse irradiates on metallic material, the coating on surface of material vaporized rapidly, forming plasma, the plasma exploded to induce a high pressure shock wave. Which can modify the microstructure of material superficial layer and results in a high compressive residual stress in material superficial layer? So that LSP can improve some mechanical properties of metallic materials, It has been proposed as a competitive alternative technology to classical treatments for improving fatigue, corrosion and wear resistance of metals (See *et al.*, 2002). LSP can effectively strengthen materials without changing chemical components of material surface. Especially can prolong the fatigue life of metallic materials such as aerospace industry, automotive engineering and internal combustion engine manufactory and so on.

Studies show that the numerical simulation method realized the forecast of residual stress to the traditional peening technology successfully, such as laser peening, ultrasonic peening, water jet peening and water-jet cavitation peening. Meguid *et al.* (1999) the elastoplastic behavior of a single projectile's interaction with metal materials in the traditional simulation shot

peening technology obtain the distribution of residual stress. HU and YE predicted the size and distribution of residual stress in the process of the laser shock peening technology by the finite element method (Hu *et al.*, 2006; Ding and Ye, 2006).It offered a new effective approach to optimize parameters of laser shock. From then on, several researchers have used ansys to analyze the laser generated shock waves propagating into different metal materials in the past six years (Braisted and Brockman, 1999; Ding and Ye, 2003; Peyre *et al.*, 2003; Ocana *et al.*, 2007; Zhang *et al.*, 2004). This research is on the basis of the test conditions of laser shock processing to SAE1070 steel, the use of ANSYS/LS-DYNA analysis platform, it establishes the appropriate finite element model of nonlinear dynamics in the technological process and the grid partition, load size, loading history and other key conditions were considered when to simulate the distribution of compressive residual stress field. And compared with the residual stress distribution which determined by X-ray diffraction method finally.

LASER SHOCK PROCESSING TEST OF SAE1070 STEEL AND PRINCIPLE OF STRENGTH

The SAE1070 steel is irradiated by a spot which diameter is 7 mm, the laser power density is 8 GW/cm² and duration is 50 ns. A section of the material to be peened is coated with paint and a thin film of water is run over the surface. A high

Corresponding Author: Bing Han, School of Mechanical Engineering and Automation, University of Science and Technology
Liaoning, Anshan 114051, China

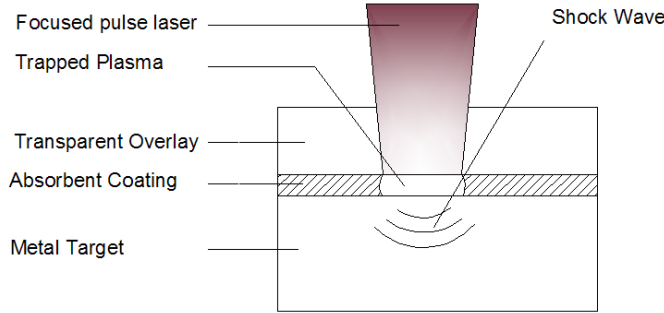


Fig. 1: Schematic of the LSP

energy laser is aimed at a particular location on the target. A single pulse sent from the laser passes through the water layer and causes the paint layer to vaporize into plasma. As the plasma expands, high pressure, short duration shock waves proceed into the water and the base metal. The presence of the water film tends to confine the energy and increase the intensity of the pressure pulse within the base. The process used to laser shock peen a target material is shown in Fig. 1. The method is similar to Ballard (1991a) investigated into LSP effects on the residual stress field and fatigue behavior of steel in his doctoral dissertation. To determine peeling and corrosion in samples, as well as residual stress distribution in terms of depth, the samples are polished with electrolytic polishing devices (Proto Electrolytic polisher-Model 8818). Stresses generated on the specimen surface were measured by X-ray diffraction and the plastically affected depths were evaluated using successive electrolytical polishing and X-ray diffraction.

FINITE ELEMENT SIMULATION

Explicit finite element algorithm: Much experimental work has been performed with regard to LSP, but relatively little effort has been spent in the development of analytical techniques to predict the residual stresses from LSP. In order to analyze the response of the material to the shock pressure with the explicit finite element method, the dynamic equation at time t can be expressed as follows, according to the virtual work principle:

Greatly LSP has extensive applied foreground in some modern manufacturing:

$$\int_{\Omega} \rho \ddot{\mu}_i \delta \mu_i d\Omega + \int_{\Omega} \nu \rho \dot{\mu}_i \delta \mu_i d\Omega$$

$$= \int_{\Omega} f_i \delta \mu_i d\Omega + \int_{\Gamma} \delta \mu_i d\Gamma - \int_{\Omega} \sigma_{ij} \delta D_{ij} d\Omega \quad (1)$$

where,

- ρ = Mass density
- $\ddot{\mu}$ and $\dot{\mu}$ = Nodal acceleration and velocity, respectively
- ν = The damping coefficient
- $\delta \mu$ = The virtual displacement
- f_i = The body force density
- T_{Γ} = The boundary force applied on the boundary Γ
- σ_{ij} = The Cauchy stress tensors,
- $D_{ij} = \frac{1}{2} (\delta u_{ij} + \delta u_{ij})$ = Deformation rate tensors.

Discretization of this problem is accomplished by means of the standard finite element procedure. After aggregation, we have the dynamic equilibrium equation as follows:

$$M \ddot{U} + C \dot{U} + F^{\text{int}} = F^{\text{ext}} \quad (2)$$

where, M is the diagonal mass matrix, \ddot{U} and \dot{U} the nodal acceleration and velocity vector, respectively, C diagonal damping matrix, F^{int} the internal element force vector, F^{ext} accounts for external and body force loads. To advance to time t_{n+1} , central difference time integration is usually used as follows:

$$\ddot{U} = M^{-1} (F^{\text{ext}} - F^{\text{int}} - C \dot{U}) \quad (3)$$

$$\dot{U}^{n+\frac{1}{2}} = U^{n-\frac{1}{2}} + \ddot{U}^n \Delta t^n \quad (4)$$

$$U^{n+1} = U^n + \dot{U}^{n+\frac{1}{2}} \Delta t^{n+\frac{1}{2}} \quad (5)$$

where,

$$\Delta t^{\frac{n+1}{2}} = \frac{(\Delta t^n + \Delta t^{n+1})}{2}$$

Then we update the geometry by adding the displacement increments to the initial geometry:

$$X^{n+1} = X^0 + U^{n+1} \quad (6)$$

The central difference scheme is conditionally stable. The stability limit can be defined using the element length L_e and the wave speed of the material C_d :

$$\Delta t_{\text{stable}} = \frac{L_e}{C_d} \quad (7)$$

The material constitutive model: Assuming that the model is an ideal elastoplastic material, it obeys the Mises yield criterion following an elastic strain constitutive relation. The highest elastic stress level in the direction of the shock wave propagation is defined as the Hugoniot Elastic Limit (HEL). At pressures greater than the HEL, permanent deformation occurs. If it is assumed that the yielding occurs when the applied stress is greater than HEL, material yield occurs. The dynamic yield strength of the material is Han and Ju (2009):

$$\sigma_y = \text{HEL} \frac{(1-2\nu)}{(1-\nu)} \quad (8)$$

where, ν is Poisson's ratio. Since the HEL is not strain-rate dependent, it is possible to determine an upper limit on the dynamic yield strength. HEL data for many materials are published in the open literature or can be obtained from flyer plate testing.

Ballard developed a one-dimensional analytical model to predict the surface residual stress induced by LSP in an elastic-plastic half-space. The model was assumed to be ax symmetric since the pressure impacts on the center of the material surface. According to Hook's law, the surface plastic strain is:

$$\varepsilon_p = \frac{-2\text{HEL}}{3\lambda + 2u} \left(\frac{P}{\text{HEL}} - 1 \right) \quad (9)$$

where, P is the impact wave pressure; u and λ are Lame's constants.

The mechanical performance parameters of the 45 steel used in the ideal elastic-plastic model are shown in Table 1.

Table 1: Performance parameters of SAE1070 steel

Properties	Value
Density, ρ/kgm^3	7.80×10^3
Poisson's ration, ν	0.28
Elastic modulus, E/GPa	2.10×10^5
Dynamic yield strength, σ_y/MPa	1.15×10^3

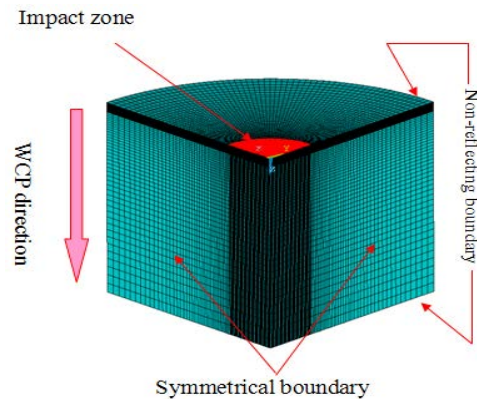


Fig. 2: Finite element model boundary conditions schemes

Finite element model: A finite element analysis method adopting LS-DYNA and ANSYS is described in detail to attain the simulation of single and multiple laser shock processing. The simulation is composed of two distinct parts including dynamic analysis performed by LS-DYNA and static analysis performed by ANSYS. The physical model in the experiment and influence of the reduced impact wave on the edge are shown in Fig. 2. A 40 mm high and 40 mm wide quarter cylinder model is established. Solid 164 is used to mesh in the model. The 10 mm length of the impact zone is divided along the X and Y directions into an average of 30 portions, with a size proportion of 1. The rest of the model is also divided into 50 portions, with a size proportion of 0.2. A 2 mm deep portion of the impact zone is divided into an average of 30 components, with a size proportion of 1. The remaining portion is divided into 60 parts, with a size proportion of 0.2. Thus, the model is divided into 436292 elements. The two sections of the model are set with a symmetrical boundary and the side and underside of the model are set with a no reflection boundary (Fig. 2). These conditions enable the transmission of the stress wave in the boundary and subsequent simulation of a 3D semi-infinite entity. Boundary conditions are incorporated into the model in accordance with the analysis of the model boundary conditions.

The spatial and temporal distribution of the pressure pulse on the surface of the target material has significant experimental efforts. For a constant laser power density I_0 , the peak pressure P is given by Fabbro *et al.* (1998).

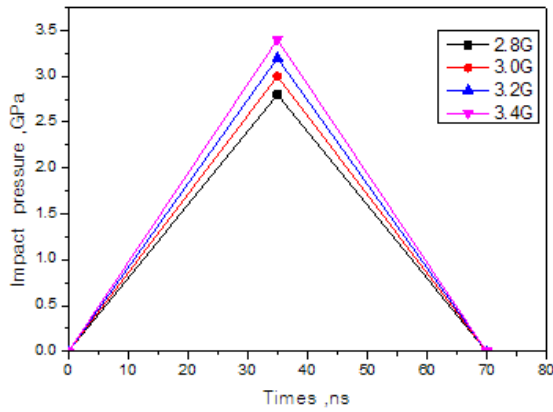
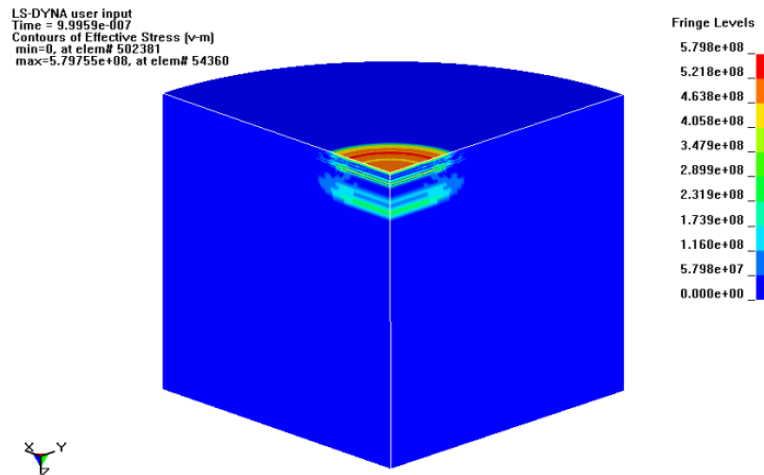


Fig. 3: Impact wave pressure changes as a function of time

$$p(GPa) = 0.01 \sqrt{\frac{\alpha}{2\alpha+3}} \sqrt{Z(gcm^{-2}s^{-1})} \sqrt{I_0(GWcm^{-2})} \quad (10)$$

where, Z is the reduced acoustic impedance [$2/Z \approx 1/Z_1 + 1/Z_2$] of the confining (Z_1) and target (Z_2) materials and α is the efficiency of the interaction. It was also reasonably assumed that 10% ($\alpha = 0.1$) of the incident energy density is used for the pressure rise of the plasma. The peak pressure is independent of the laser pulse duration or the laser wavelength but is proportional to the square root of the laser pulse intensity. The surface residual stress can be expressed as Ballard (1991b)

$$\sigma_{surf} = \sigma_0 - \left[\frac{\mu \epsilon_p (1+\nu)}{(1-\nu)+\sigma_0} \right] \left[1 - \frac{4\sqrt{2}}{\pi} (1+\nu) \frac{L_p}{r_p \sqrt{2}} \right] \quad (11)$$



(a) $t = 999$ ns

where, σ_0 = The initial surface residual stress and is set as zero in this study.

Impact wave load, method and loading time during WCP are key factors that determine the accuracy of numerical simulations. The duration of impact waves is 70 ns. The variations in the impact wave pressure as a function of time are shown in Fig. 3.

RESULTS OF LASER SHOCK PROCESSING AND DISCUSSION

Dynamics analysis: In the post processor of ANSYS/LS-DYNA, the impact waves are dynamically propagated in the finite element model. The von Mises stress of impact wave propagation in the finite element model at different periods is shown in Fig. 4. According to the stress wave theory, the elastic wave velocity and the plastic wave velocity can be calculated as follows Wang (1985):

$$C_l^e = \sqrt{\frac{(1-\nu)E}{(1+\nu)(1-2\nu)}} \cdot \frac{1}{\rho} \quad (12)$$

$$C_l^p = \sqrt{\frac{E}{3(1-2\nu)}} \cdot \frac{1}{\rho} \quad (13)$$

where,

- c_l^e = The elastic wave velocity
- c_l^p = The plastic wave velocity
- ρ = The material density
- E = The Elastic modulus
- ν = The Poisson's Ratio

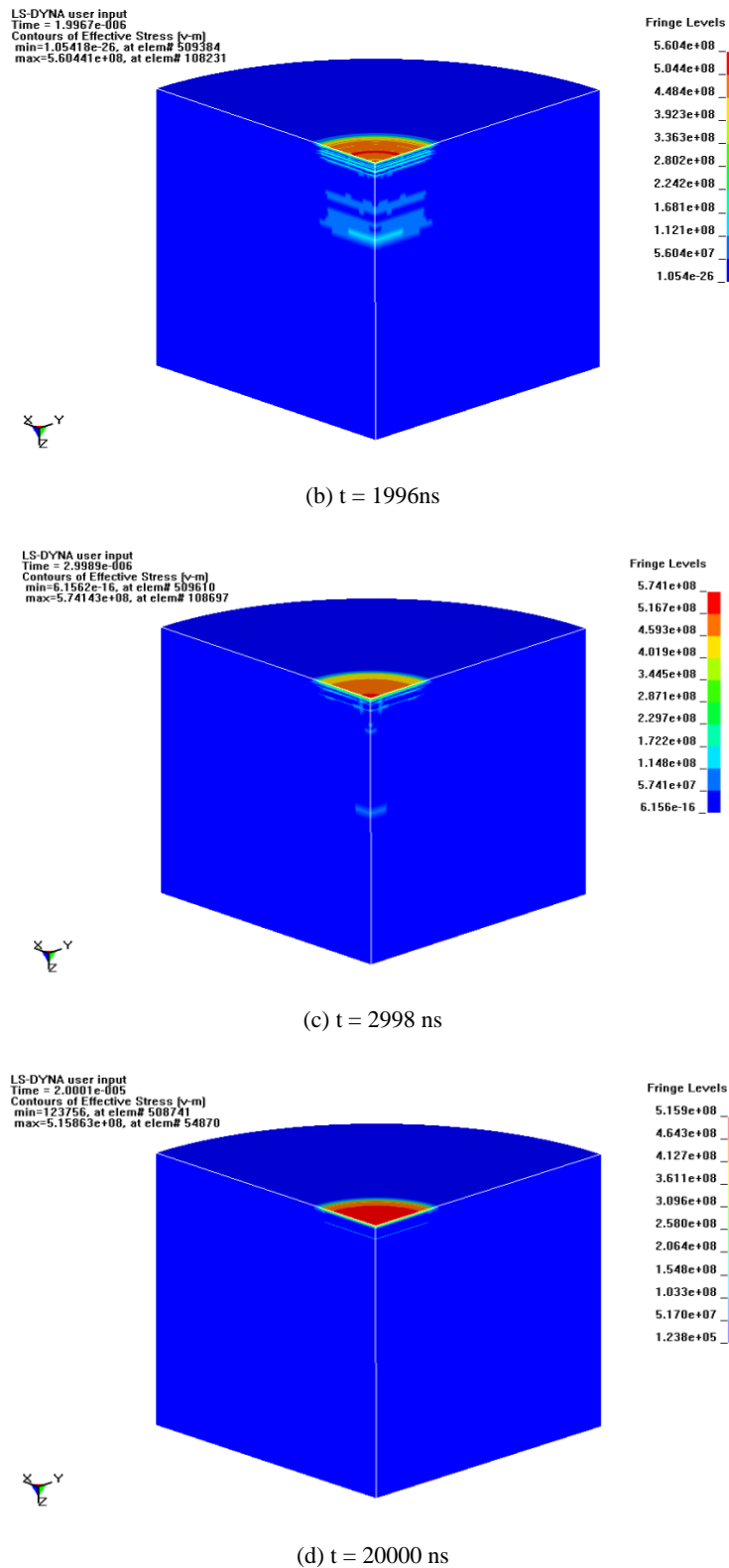


Fig. 4: The dynamic stress wave propagation process

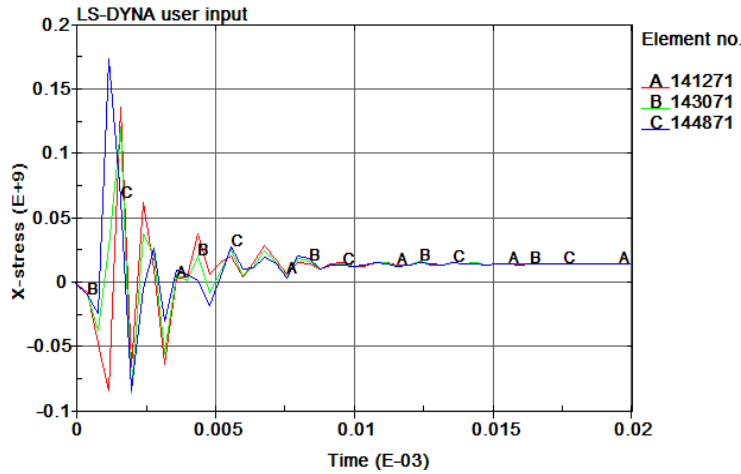


Fig. 5: Residual X-stress dynamic change as a function of time at different element

It is easy to find that the elastic wave velocity is always faster than the plastic one. Then time needed for the first two types of stress wave propagating to the bottom surface of the target material is shown as follows:

$$t_e = \frac{l_{\text{thick}}}{c_l^e} \quad (14)$$

$$t_p = \frac{l_{\text{thick}}}{c_l^p} \quad (15)$$

where, l_{thick} is the thick of target material.

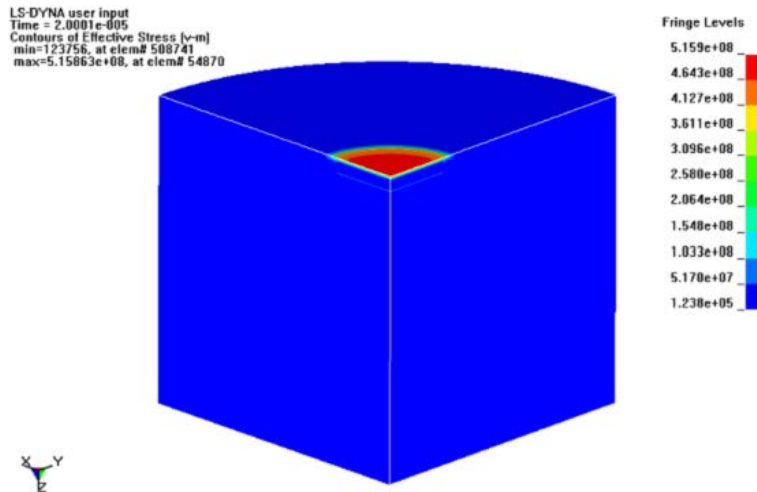
The impact wave spreads from the surface inward and then to the bottom, with a maximal von Mises stress of 579 MPa (Fig. 4a). The maximal von Mises stress of the finite element model decreases to 560 MPa when 1996 ns (Fig. 4b). The impact wave spreads to the center of the finite element model, the energy gradually increases with depth and the maximum von Mises stress decreases to 574 MPa (Fig. 4c). The internal impact wave and continuous interaction of the material continuously increases the energy, eventually forming a stable residual stress field on the surface of the model. The maximal von Mises stress is 515 MPa (Fig. 4d).

The X-dynamic process of different typical units (element no.: 141271, 143071, 144871) on the material surface after five continuous cycles of impact waves is shown in Fig. 5. When the material is subjected to five impact waves, element stress shocks occur between compressive and tensile stresses, which become stable after approximately 20000 ns, with a maximum

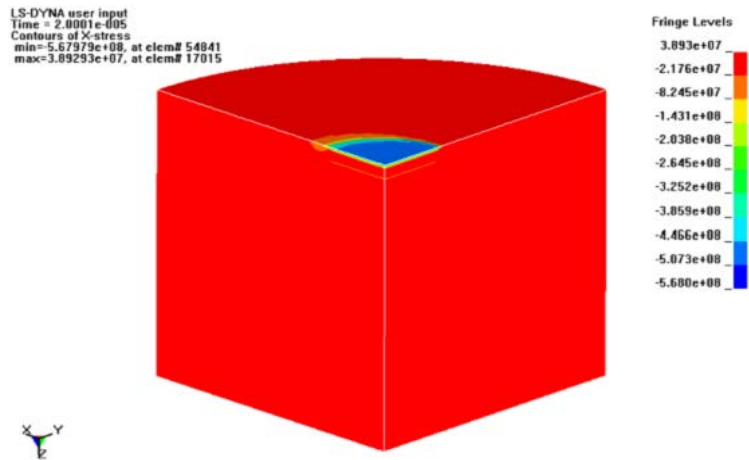
amplitude of approximately 300 MPa. Residual stress continuously increases after each impact wave.

Final formation of residual stress: The residual stress distribution formed near the surface is depicted in Fig. 6, x and y components of residual stresses are only produced in the layer about 1 mm from the top surface after laser shock processing. The residual stress is symmetrically distributed along the X and Y directions and has a consistent value (Fig. 6b and 6c) and z component of stress is nearly zero on the top surface. A tensile residual stress is found in the z component of stress of the model as shown in Fig. 6d, which is generated by the reversing yielding effect due to the interaction of the various stress waves in the material. The simulation results are consistent with the experimentally measured residual stresses. The compressive residual stress formed near the surface is approximately -389 MPa. The final equivalent stress distribution, in which the von Mises stress reaches 515 MPa, is illustrated in Fig. 6a.

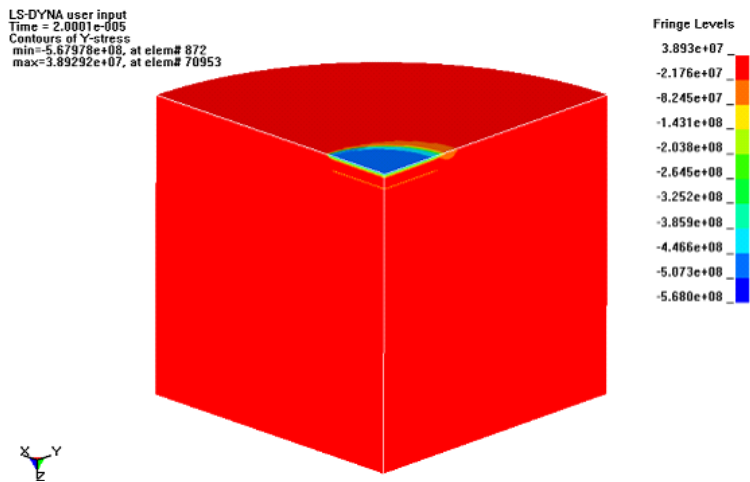
Influence of different peak loads on residual stress: To determine the varying patterns of residual stress of different nodes along depths with increasing shock waves, The varying patterns of the elements along the impact direction with shock waves and under continuously varying peak values are shown in Fig. 7. Under the different peak value loads, the varying patterns of the residual stresses of the elements with the number of shock waves are different and the residual stresses of the different elements also different. As indicated by the numerical value, the surface residual stress, after the application of the shock wave functions and a peak load $P = 2.8$ GPa, yields a maximum



(a) Contours of effective stress



(b) Contours of residual X-stress



(c) Contours of residual Y-stress

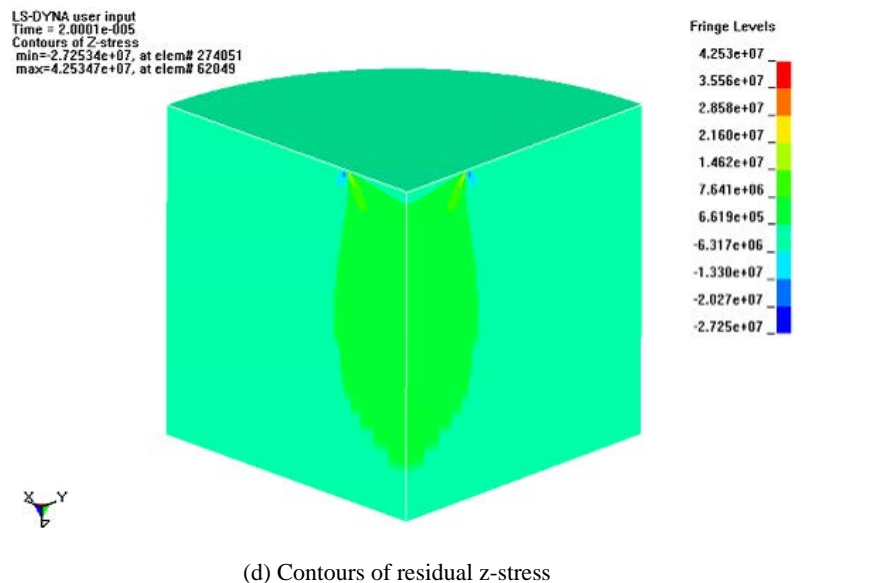


Fig. 6: Residual stress field

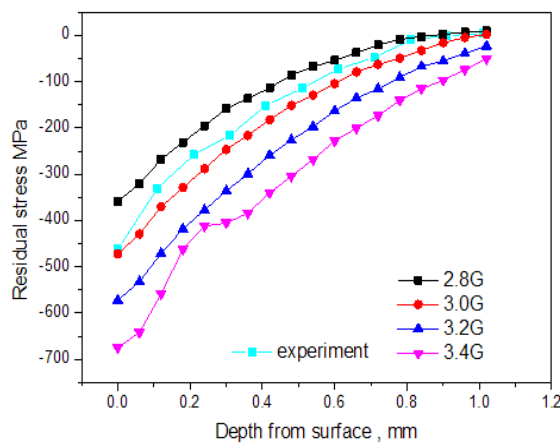


Fig. 7: Comparison with residual stress simulation and test results

compressive residual stress of approximately -359 MPa. At a peak load $P = 3.4$ GPa, the maximum compressive residual stress is approximately -675 MPa.

COMPARISON OF SIMULATION AND EXPERIMENTAL

Peak load differs after the application of the impact waves. The numerical simulation and experimental results for residual stress distribution are compared in Fig. 7: The simulation results for the residual stress near the surface from 0 to 1 mm are slightly lower than the test results, but at the beginning and the ending, the

numerical simulation is a little lower than experimental results, broadly speaking, the simulation results for peak load is 3.0 GPa and the experimental results of 50ns shot peening show high consistency.

CONCLUSION

- A finite element analysis method adopting ANSYS and LS-DYNA is described in detail to attain the simulation of single and multiple laser shock processing and a bilinear isotropic model in a nonlinear inelastic model is created. The residual stress distribution on the surface layer of SAE1070 steel during LSP under different peak loads can be obtained.
- On top surface of the material treated, a homogeneous depression with little roughness modification in the action zone of the shock pressure is induced by single LSP, according to the simulation of surface deformation. The simulation of residual stress field for single laser shock is found to be well correlated with the experimental data and indicates that compressive residual stress of the material is approximately uniform on shocked region and the stress gradient in depth is small.
- The simulation results under peak loads of 3.0GPa, agree well with the experimental results. Thus, the ANSYS/LS-DYNA analysis platform can be used to predict the residual stress distribution induced by LSP.

REFERENCES

- Ballard, P., 1991a. Residual stressed induced by rapid impact-applications of laser shocking. MA Thesis, Palaiseau, Ecole Poly Technique, France.
- Ballard, P., 1991b. Residual stresses induced by rapid impact-applications of laser shocking. Ph.D. Thesis, Ecole Poly Technique.
- Braisted, W. and R. Brockman, 1999. High spatial resolution: High energy synchrotron x-ray diffraction characterization of residual strains and stresses in laser shock peened inconel 718SPF alloy. *Int. J. Fatigue*, 21: 719.
- Ding, K. and L. Ye, 2003. Three-dimensional dynamic finite element analysis of multiple laser shock peening processes. *Surf. Eng.*, 19(5): 351-358.
- Ding, K. and L. Ye, 2006. Simulation of multiple laser shock peening of a 35CD4 steel alloy. *J. Mater. Proc. Technol.*, 178(1-3): 162-169.
- Fabbro, R., P. Peyre, L. Berthe and X. Scherpereel, 1998. Physics and applications of laser-shock processing. *J. Laser Appl.*, 10(6): 265-279.
- Han, B. and D.Y. Ju, 2009. Compressive residual stress induced by water cavitation peening: A finite element analysis. *Mater. Design*, 30(8): 3325-3332.
- Hu, Y.X., Z.Q. Yao and J. Hu, 2006. 3-D FEM simulation of laser shock processing. *Surf. Coatings Technol.*, 20(3-4): 1426-1435.
- Meguid, A.S., G. Shagal and J.C. Stranat, 1999. Finite element modeling of shot-peening residual stresses. *J. Mater. Proc. Technol.*, 92(93): 401-404.
- Ocana, J.L., M. Morales, C. Molpeceres, O. García, J.A. Porro and J.J. García-Ballesteros, 2007. Short pulse laser microforming of thin metal sheets for MEMS manufacturing. *Appl. Surf. Sci.*, 254(4): 997-1001.
- Peyre, P., A. Sollier, I. Chaieb, L. Berthe, E. Bartnicki, et al., 2003. Analysis of laser shock waves and resulting surface deformations in an Al-Cu-Li aluminum alloy. *Eur. Phys. J. Appl. Phys.*, 23: 83-88.
- See, D.W., J.L. Dulaney, A.H. Clauer, et al., 2002. Laser peening without coating: Process, effects and applications. *Surf. Eng. Appl. Electrochem.*
- Wang, L., 1985. Stress Wave Theory. Beijing, Post and National Defense Industry Publisher, China.
- Zhang, W., Y.L. Yao and I.C. Noyan, 2004. Microscale laser shock peening of thin films, Part 2: High spatial resolution material characterization. *J. Manuf. Mater. Sci. Eng.*, 126: 18-24.